Pergamon

Journal of Structural Geology, Vol. 16, No. 3, pp. 337 to 354, 1994
Elsevier Science Ltd
Printed in Great Britain
0191-8141/94 $06.00+0.00

Kinematic analysis of a large-scale leading edge fold, Lost River Range, Idaho

DONALD M. FISHER

Department of Geosciences, Pennsylvania State University, University Park, PA 16802, U.S.A.

and

DAVID J. ANASTASIO

Department of Earth and Environmental Sciences, Lehigh University, Bethlehem, PA 18015, U.S.A.

(*Received* 6 *July* 1992; *accepted in revised form* 20 *May* 1993)

Abstract—The Mahogany Creek–Buck Creek structure within the Lost River Range, Idaho, is a large-scale, leading edge fold which developed in late Paleozoic outer shelf stratigraphy during the Sevier orogeny. Incremental strain histories determined from antitaxial fibrous pressure shadows are used to quantify temporal variations in the magnitude and orientation of elongation as a function of structural position around the leading edge of this northward and eastward propagating blind thrust. Plane strain is indicated by coaxial, up-dip extension on cleavage planes. On the backlimb of the structure, the Bluebird Mountain Formation, a calcareous sandstone, has deformed by flexural-flow whereas the forelimb of the structure records spin through a fixed steeply plunging incremental extension direction. The flat limb ahead of the anticline exhibits top-to-the-foreland simple shear. In contrast, the underlying Surrett Canyon Formation, a thick-bedded limestone, has experienced flexural-flow localized within thin zones on both limbs of the anticline. Samples from the anticlinal hinge zone suggests kinematic partitioning with pin lines which were variably distributed within each unit and which were temporally transient. Finite elongations are greatest in the hinge and above the foreland flat in the Bluebird Mountain Formation but are negligible in the Surrett Canyon Formation, except within the mechanically active interbeds of the hanging wall and within the footwall adjacent to the fault along the northernmost exposures. Strain histories in the hanging wall do not vary significantly along strike, while the footwall varies from undeformed in the south to penetratively deformed in the north. Thus, the strain data are consistent with self-similar along-strike fold development in the hanging wall during strike-parallel ramp propagation. Forward thrust propagation may have been blunted by a combination of fold-accommodated shortening and footwall deformation to the north. Once the fold had tightened and fold shortening required greater differential stress, forward fault propagation resumed, transporting the anticline onto the upper flat with little change in hanging wall fold geometry or strain distribution.

INTRODUCTION

THE relationship between folding and faulting in thrust belts can be described in terms of geometry, timing, kinematics and mechanics. Based on geometry, fold–fault relationships can be classified into three types: (1) folds that coincide with the leading edge or tip line of a thrust, e.g. ductile bead folds, leading edge folds, blind-thrust anticlines, décollement thrusts, tip anticlines, break-thrust folds or fault-propagation folds (Elliott 1976, Boyer 1986, Jamison 1987, Geiser 1988, Mitra *et al.* 1988, Suppe & Medwedeff 1990, Fischer *et al.* 1992); (2) folds that develop along flat segments of the fault surface, e.g. décollement folds, detachment folds, intraplate folds or lift-off folds (Namson 1981, Jamison 1987); and (3) folds that develop above non-planar segments of the fault surface, e.g. ramp anticlines, fault bend folds or trailing edge folds (Boyer & Elliott 1982, Suppe 1983, Boyer 1986, Jamison 1987). All of these classifications for thrust-related folds are used to define a structural geometry, but several also have kinematic or mechanical implications that have yet to be tested for large-scale natural structures.

The difficulty with testing kinematic models arises from the fact that fold–fault geometry and finite strain measurements do not uniquely constrain the kinematics or the displacements that lead to the deformed state. The displacement field during folding and thrust sheet emplacement is controlled by the imposed boundary conditions and consists of translation parallel to the underlying fault and internal strain that reflects displacement gradients within the thrust sheet. Much of the internal deformation within thrust sheets may be characterized by layer-parallel simple shearing or gradients in layer-parallel velocity normal to layering (Suppe 1983, Geiser *et al.* 1988, Wojtal & Mitra 1988). In a folded thrust sheet these gradients are defined by the existence, distribution and temporal evolution of pin lines (or lines of no interbed shear) (Fig. 1). Lateral gradients in layer-perpendicular and layer-parallel velocity components are related to variation in slip on bounding fault surfaces, and the entire thrust sheet may be subject to global pure shear or layer-parallel shortening. Thus, the determination of fold–fault kinematics requires an evaluation of finite strain gradients as well as the distribution of incremental strain histories (i.e. the spatial and temporal variation in the layer-parallel shear strain) relative to a well-constrained structural geometry.

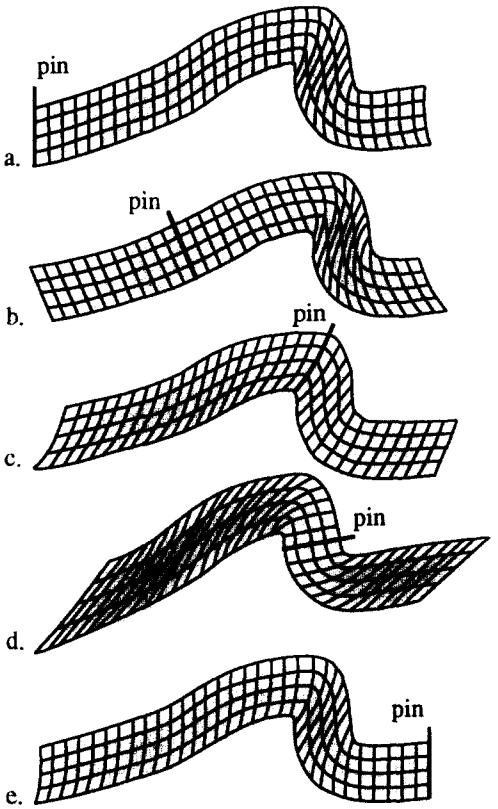

Fig. 1. Diagram showing effect of pin position on distribution of layer-parallel shearing within a layer for given fold geometry (from Geiser *et al.* 1988). The grid was constructed by laying off equally spaced lines in the deformed state measured from a pin perpendicular to layering. Patterns represent deformation of an originally orthogonal grid. Vertical lines of deformed grid are loose lines. Horizontal lines are shape of the Nugget sandstone in the Yellow Creek anticline, with additional lines determined by parallel projection downward.

One approach to the determination of kinematics is to evaluate spatial variations in finite strain and geometry in a laterally continuous structure (Spratt 1987). In this case, the assumption is made that space can be substituted for time. The incremental strain history, or the sequence of displacements that produced the deformed state, is reconstructed by considering the series of strain increments that would lead to the measured spatial variation in the orientation and magnitude of the finite strain ellipse. An alternative approach is to measure the incremental strain histories using syntectonic fibers from different localities along a cross-section of a structure and to infer the temporal evolution in fold geometry that is most consistent with the distribution of strain histories (Beutner & Diegel 1985). In this paper we present incremental and finite strain histories for samples from two valleys that cut through a laterally continuous anticline at the leading edge of a kilometer-scale thrust sheet in the Lost River Range, Idaho. This methodology allows for the independent evaluation of kinematics at different positions along the hinge line of the structure. No time–space equivalence is assumed, and lateral variations in structural evolution are characterized. The distribution of strain histories is used to evaluate the position and temporal evolution of pin lines as well as the importance of lateral strain gradients at the leading edge of the thrust sheet.

GEOLOGIC SETTING

North of the Snake River plain, in east-central Idaho, the Sevier-age thrust belt is broken into several NNE-trending ranges separated by Tertiary basins (Ruppel & Lopez 1984) (Fig. 2). Our study is concentrated on structures within Mississippian and Pennsylvanian strata in the northern Lost River Range, just east of the deformed positions of the Mississippian shelf edge and the Antler orogenic front and well to the hinterland of the Sevier thrust front. The regional structure of the northern Lost River Range is a synclinorium, with the lower part of the section exposed along the western, northern and eastern flanks of the range and the younger units exposed within the core (Fig. 3). Within this synclinorium, the section is folded into a series of large-scale, Sevier-age folds which are spectacularly exposed in glacial valleys with up to 1000 m of topographic relief (Fig. 4). First-order folds within upper Paleozoic strata are disharmonic with respect to structures involving the lower Paleozoic section. These upper Paleozoic strata include the McGowan Creek, Middle Canyon, Scott Peak, South Creek, Surrett Canyon, Arco Hills, Bluebird Mountain and the Snaky Canyon Formations (Ross 1947, Mapel *et al.* 1965, Skipp & Hait 1977, Skipp *et al.* 1979a, Sandberg *et al.* 1982) (Fig. 4). Depth-to-

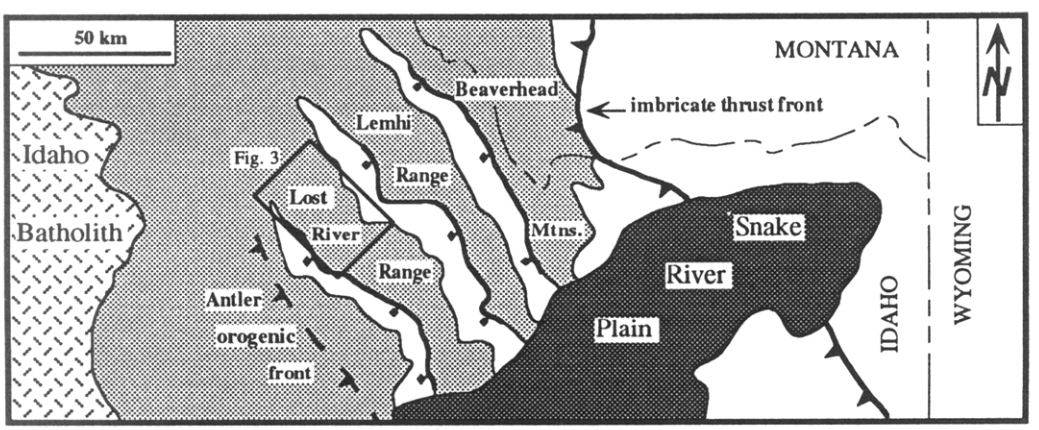

Fig. 2. Location map of the study area showing the position of the Lost River Range, Idaho, within the Rocky Mountains.

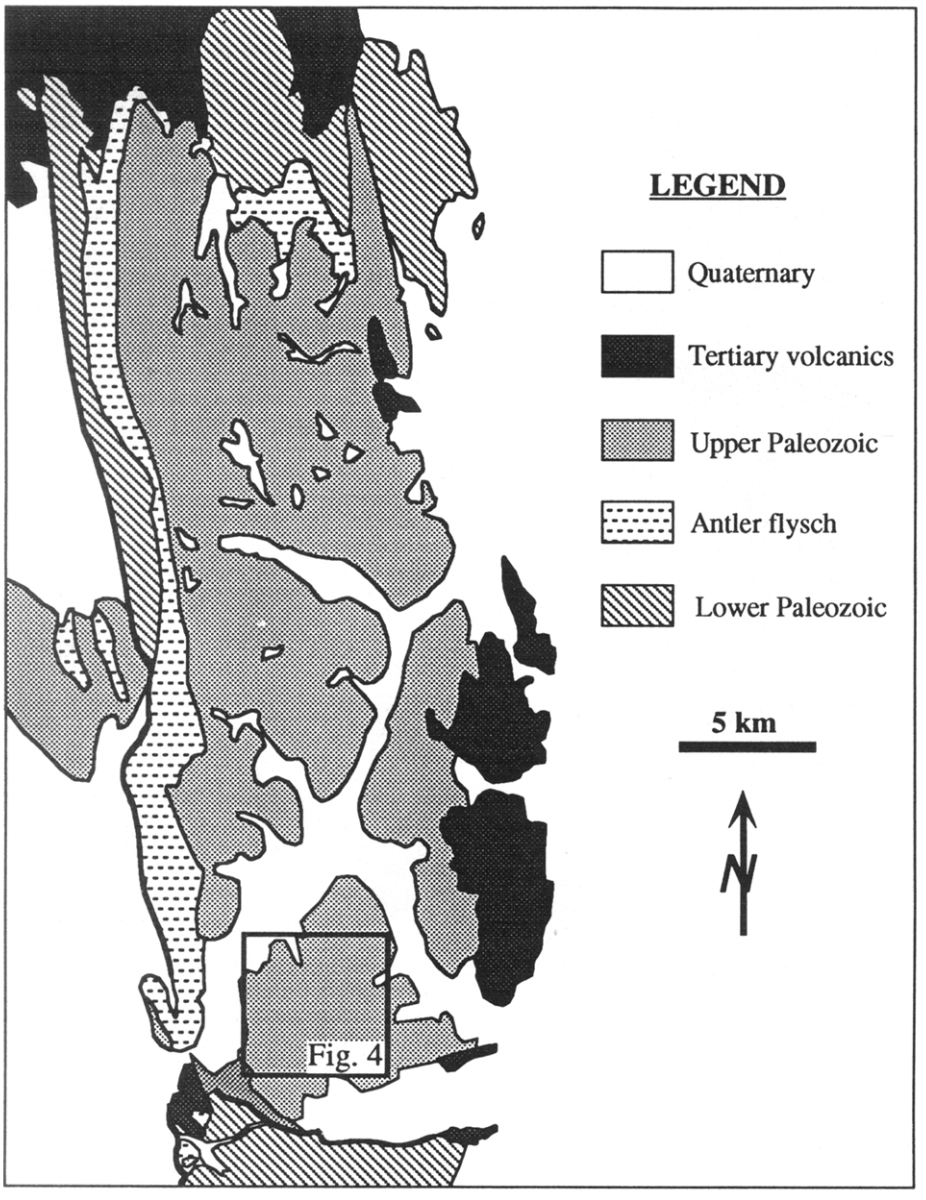

Fig. 3. Generalized geologic map of the northern Lost River Range.

detachment calculations using down-plunge projections of these folds suggest a regional detachment at the base of the McGowan Creek Formation. Each unit above this detachment exhibits a different structural style during deformation. The South Creek Formation, for example, is in some cases tightly folded into mesoscopic conjugate folds and disharmonic folds, and was clearly detached from the surrounding, stiffer Scott Peak and Surrett Canyon Formations. Illite crystallinity determinations in the Scott Peak Formation are consistent with a peak temperature of approximately 220°C.

Variations in structural style within the range reflect differences in lithology and layer thickness. The McGowan Creek Formation, which varies from 1100 to 300 m thick from the western to eastern margins of the northern Lost River Range (Mapel *et al.* 1965, Skipp *et al.* 1979b), consists of distal turbidites shed eastward off the uplifted Antler highlands in the early Mississippian (Sandberg 1975). Much of the remainder of the late Paleozoic stratigraphy in eastern Idaho records the build up of a westerly prograding carbonate shelf complex (Rose 1977, Skipp *et al.* 1979b, Sandberg *et al.* 1982). Our strain measurements are from the Surrett Canyon, Arco Hills, Bluebird Mountain and Snaky Canyon Formations. The Surrett Canyon Formation is a 260–335 m package of thick-bedded fossiliferous limestone with some clastic interbeds (Mamet *et al.* 1971). Within the clastic interbeds, a steeply dipping penetrative cleavage is defined by stylolytic to anastomosing dark seams around matrix-supported quartz grains. Massive fossiliferous beds in the Surrett Canyon Formation are uncleaved. The overlying Arco Hills Formation is a chert-rich unit with some clastic interlayers that display a cleavage defined by short, dark, discontinuous seams and a grain shape fabric related to matrix calcite grains. The Bluebird Mountain Formation is a fine-grained calcareous sandstone composed of a micritic matrix and angular, 30–100 μm matrix- to framework-supported quartz grains. Throughout the Bluebird Mountain Formation, a penetrative cleavage is steeper than bedding

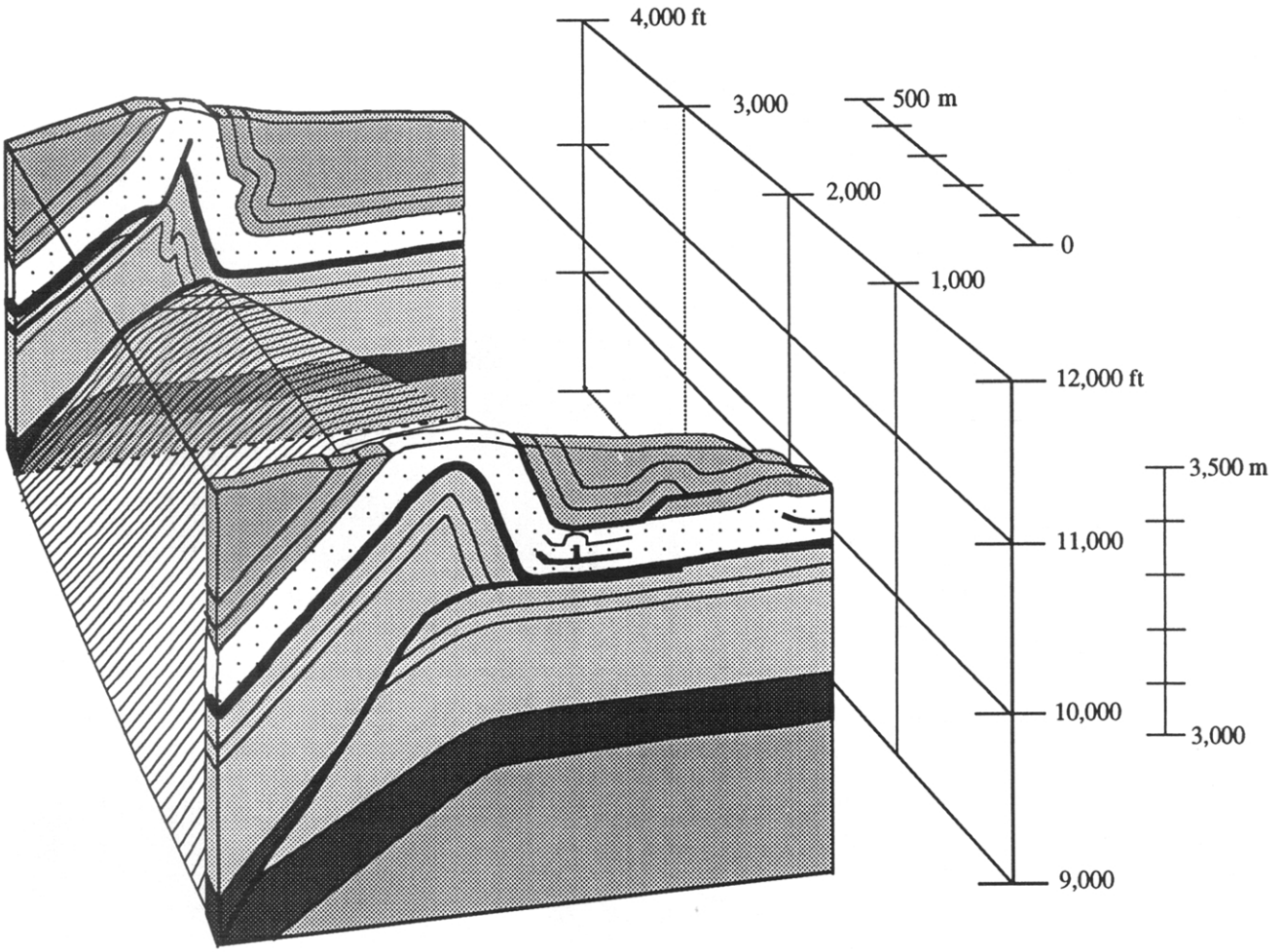

Fig. 5. Perspective view to north of Mahogany Creek and Buck Creek sections illustrating geometry of the blind-thrust complex. Information from Mahogany Creek and Buck Creek valleys and intervening ridge are projected onto section lines shown in Fig. 4. Patterning is also same as in Fig. 4.

and refracts through layers of variable grain size. This cleavage is defined by the grain shape fabric associated with matrix calcite grains as well as discrete, anastomosing seams that are localized at the margins of quartz grains. The Snaky Canyon Formation, deposited in the early Pennsylvanian–early Permian, overlies the Bluebird Mountain Formation and consists of interbeds of sandstone–siltstone with an anastomosing cleavage and massive uncleaved carbonate.

This study is focused on the exposed leading edge of a large-scale thrust fault that developed as an out-of-syncline thrust (Dahlstrom 1970) on the eastern limb of a second-order syncline. The tip line of the thrust is exposed in two opposing valleys that provide cross-sectional views of the thrust tip (Figs. 4–6). Along the Mahogany Creek section (to the south) (Figs. 4, 5 and 6a), the fault cuts through the Surrett Canyon Formation (hanging wall ramp on footwall ramp) and becomes a flat at the base of the Arco Hills Formation (hanging wall flat on footwall flat). Displacement on this flat decreases towards a tip line which plunges ~11° to the north. The ramp anticline in the hanging wall has an interlimb angle of ~78° at the stratigraphic level of the Bluebird Mountain Formation with a smaller angle in the Surrett Canyon Formation. The fold axis plunges ~10° to the north. The back limb dip is ~45–50°, and the forelimb dip is ~65–75° with the steepest dips in the Surrett Canyon Formation. In addition, the hanging wall anticline has a chevron shape in the Surrett Canyon Formation and a box shape in the upper beds of the Bluebird Mountain Formation and, based on geometry alone, could be described as a fault propagation fold with a décollement breakthrough (Suppe & Medwedeff 1990). In the hanging wall ahead of the forelimb of the large-scale anticline, smaller-scale structures such as a décollement fold within the Bluebird Mountain Formation, a small thrust fault at the base of the Snaky Canyon Formation, and a series of small thrust faults higher in the section accommodate significant shortening (Figs. 5 and 6a). Similar features are not observed in the footwall, so these structures are likely a manifestation of the hanging wall shortening required by decreases in fault displacement near a tip line that is propagating toward the foreland (Chapman & Williams 1984).

Along the Buck Creek section (to the north) (Figs. 4, 5 and 6b), the back limb dip is ~30–45° and the forelimb dip is ~45–90° with most dip measurements around 60°. At the stratigraphic level of the Bluebird Mountain Formation, the interlimb angle is ~95°. The fault cuts up-section eastward through the Surrett Canyon Forma-

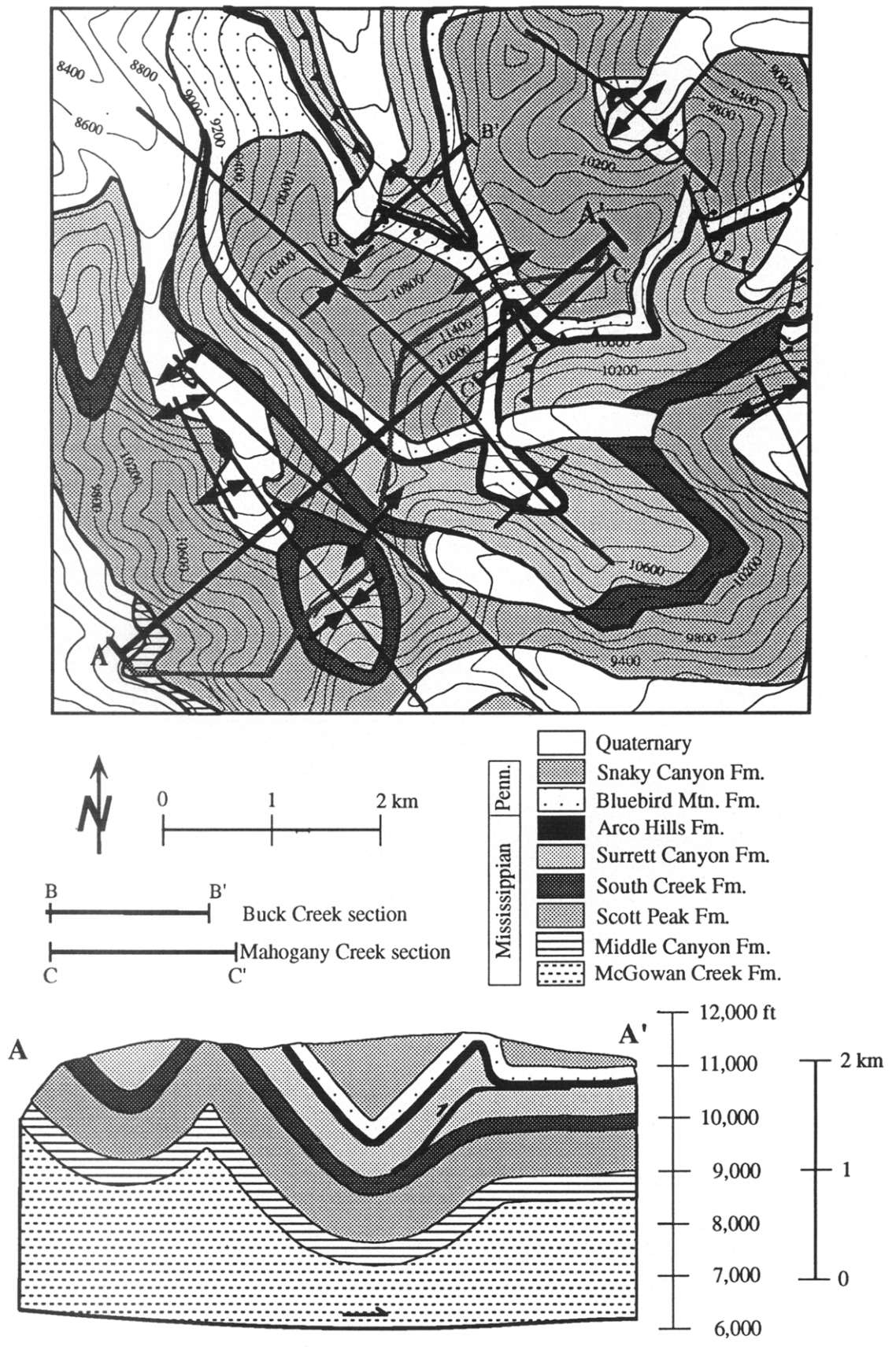

Fig. 4. Geologic map and accompanying cross-section of the Mahogany Creek and Buck Creek area. The top of the cross-section A–A′ is projected from the jagged ridge (gray line).

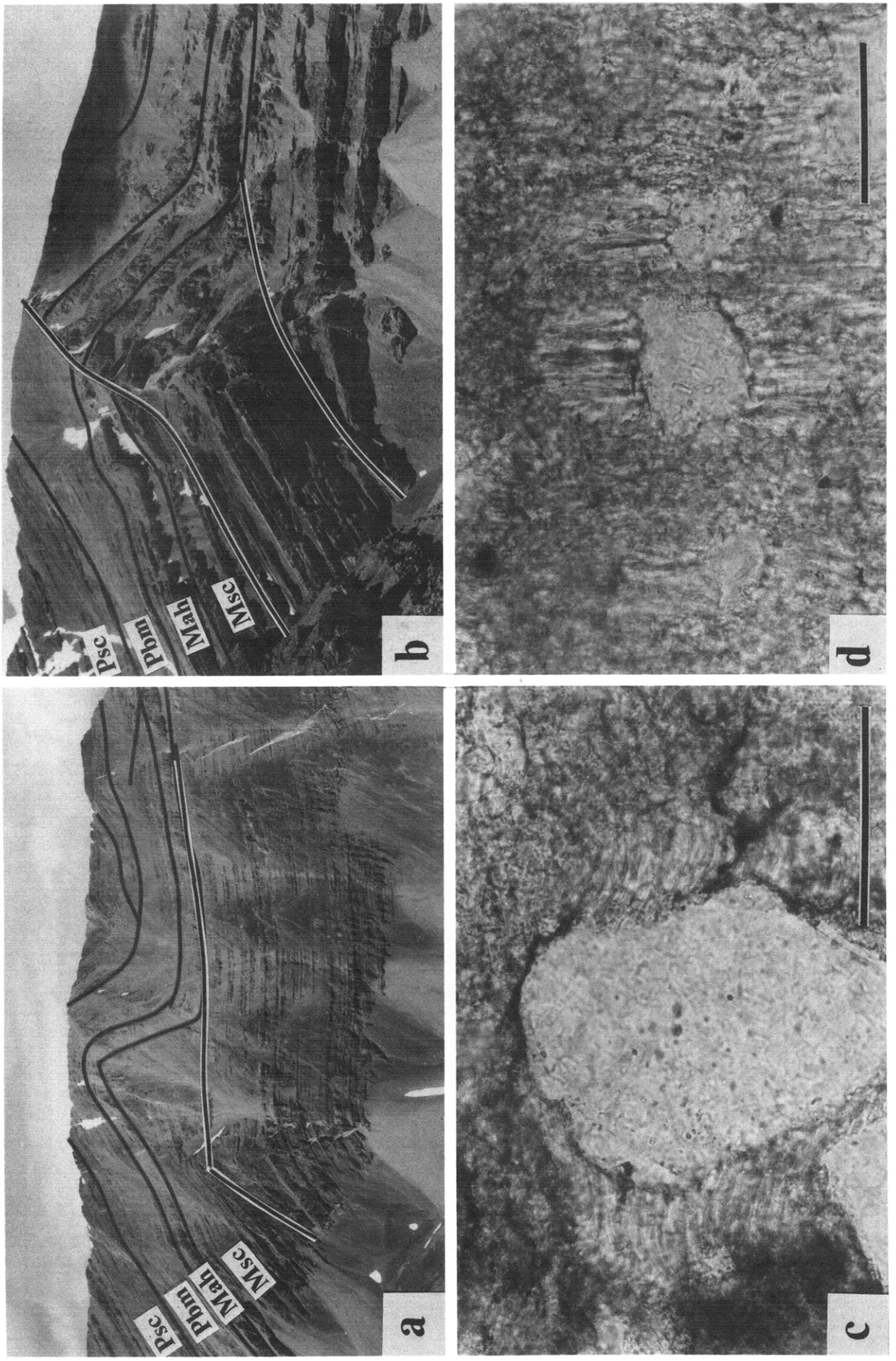

Fig. 6. Annotated photographs of (a) Mahogany Creek and (b) Buck Creek sections, view to the north. Vertical relief is ~600 m. Msc, Surret Canyon Formation; Mah, Arco Hills Formation; Pbm, Bluebird Mountain Formation; and Psc, Snaky Canyon Formation. Photomicrographs of representative pressure shadows from the northern Lost River Range showing (c) a pressure shadow observed in the *XZ* section with curved antitaxial calcite fibers from the Surret Canyon Formation (sample BC10, scale bar = 50 μm), and (d) pressure shadows observed in the *XY* section around detrital quartz grains from the Bluebird Mountain Formation (sample 124, scale bar = 50 μm).

tion (hanging wall ramp on footwall ramp) and terminates just below the contact with the Arco Hills Formation. Thus, there is greater displacement and stratigraphic separation along the fault surface and a higher stratigraphic position for the tip line towards the south (at Mahogany Creek). Based on these considerations, we argue that the thrust fault propagated laterally to the north between Mahogany Creek and Buck Creek during eastward motion (e.g. Douglas 1958).

The Lost River Range and surrounding areas experienced Tertiary and Quaternary extension after Sevier thrusting. In the southern Lost River Range, fold and thrust structures are cut by high and low angle normal faults such as the Pass Creek detachment system and the Donkey fault (Link *et al.* 1988, Janecke 1989, Janecke *et al.* 1991). In the northern Lost River Range, the thrust belt is exposed within a largely coherent normal fault-bounded block that is not dissected by numerous extensional faults (Mapel *et al.* 1965), although one listric extensional fault cuts the back limb of the Buck Creek exposure (Fig. 6b). Because we are fixing our reference frame at the scale of an individual continuous structure (i.e. the Mahogany Creek–Buck Creek structure) and because there is an absence of near-surface penetrative deformation associated with the ongoing extensional event, regional tilting and retrodeformable extensional faults do not affect our ability to evaluate the Sevier-age kinematics within this restricted region.

INCREMENTAL STRAIN ANALYSES

In this study, we have used the Durney & Ramsay (1973) 'pyrite method' to quantify strain histories based on fibrous overgrowths around rigid particles. This method assumes that fibers behave rigidly, fiber growth is antitaxial (i.e. fiber growth is directed toward the rigid particle and occurs at the interface between the rigid particle and the fibrous overgrowth), fiber growth parallels the incremental extension direction (i.e. displacement-controlled fiber growth), and individual fibers do not curve out of the plane of the thin section. The strain history for curved fibers can be approximated by a series of small increments of pure shear separated by rigid-body rotations (Elliott 1972, Wickham 1973).

Fiber behavior (i.e. deformable or rigid) is difficult to assess optically in most overgrowths because fibers are too fine-grained to test for optical continuity or micro-offsets along a curved fiber (e.g. Spencer 1991). In some cases, however, calcite overgrowths around quartz grains have nucleated on individual large fossil fragments rather than the micritic matrix. All the curved fibers in the pressure shadow are optically continuous with the seed calcite crystal. Thus, there is no evidence in these examples for bending of initially straight calcite fibers. Less common quartz fibers in pyrite pressure shadows display optical continuity or less sweep in orientation along the fiber than the observed fiber curvature. These observations suggest that the fiber curvature reflects changes in the incremental extension direction and that fibers behaved rigidly throughout the deformation. Because we cannot in most cases document or rule out the possibility of passive deformation of fibers, we have chosen to assume that all fibers grow parallel to the extension direction and that fibers subsequently behave rigidly, so that the measured strain history provides a direct representation of the fiber shape.

Several observations suggest that fiber growth is antitaxial: (1) fibers (generally calcite) are different minerals than rigid grains (quartz or pyrite) but the same minerals as the matrix (calcite) (Fig. 6c); (2) in some samples, syntaxial calcite fibers on calcareous fossil fragments (i.e. fibers optically continuous with the host calcite fragment) have an opposite sense of curvature to calcite fibers in overgrowths around detrital quartz grains and pyrite framboids; and (3) when the material adjacent to the quartz grains is coarse grained (e.g. a fossil fragment), the calcite fibers are in optical continuity with the calcite fragment. Based on these considerations, the oldest fiber material is near the matrix–overgrowth boundary and the most recent material is near the surface of the host. Observation (2) also indicates that fiber growth is displacement-controlled and not face-controlled (e.g. Ramsay & Huber 1987).

Three-dimensional geometry of pressure shadows was evaluated by considering two orthogonal sections in each sample, one cut parallel to cleavage and one cut perpendicular to cleavage and the bedding–cleavage intersection. In cleavage-parallel sections, fibers are straight or only slightly curved in all the sections, with a down-dip extension direction that is perpendicular to the subhorizontal bedding–cleavage intersection (Fig. 6d). These straight fibers indicate plane strain, with no component of fiber growth parallel to the fold axis. Thus in cleavage-perpendicular sections, fibers do not curve out of the section, and a complete strain history can be measured. In all our examples, we will refer to strain histories measured in cross-sections of the structure as viewed to the north. The tectonic transport direction is eastward, so top-to-the-foreland is equivalent to a clockwise sense of shear.

Syntectonic overgrowths provide information about the absolute elongation, but no information about the absolute shortening or the strain ratio; an independent measure of these parameters is necessary before volume changes can be quantified. At present, we are unable to assess the importance of volume change, so we emphasize that the spatial variations in magnitude of measured finite elongations could be interpreted as either variations in the ratio of the principal elongations ($\varepsilon_1/\varepsilon_3$) or variations in volume change.

The deformation history of each sample is reconstructed by digitizing the trace of bedding, the center of the rigid host and a central fiber from each overgrowth. These co-ordinates are used to calculate a cumulative incremental strain and a progressive finite strain history (e.g. Durney & Ramsay 1973, Wickham 1973, Fisher & Byrne 1992, Clark *et al.* 1993) (Fig. 7). In all strain history diagrams, the trace of bedding is arbitrarily used

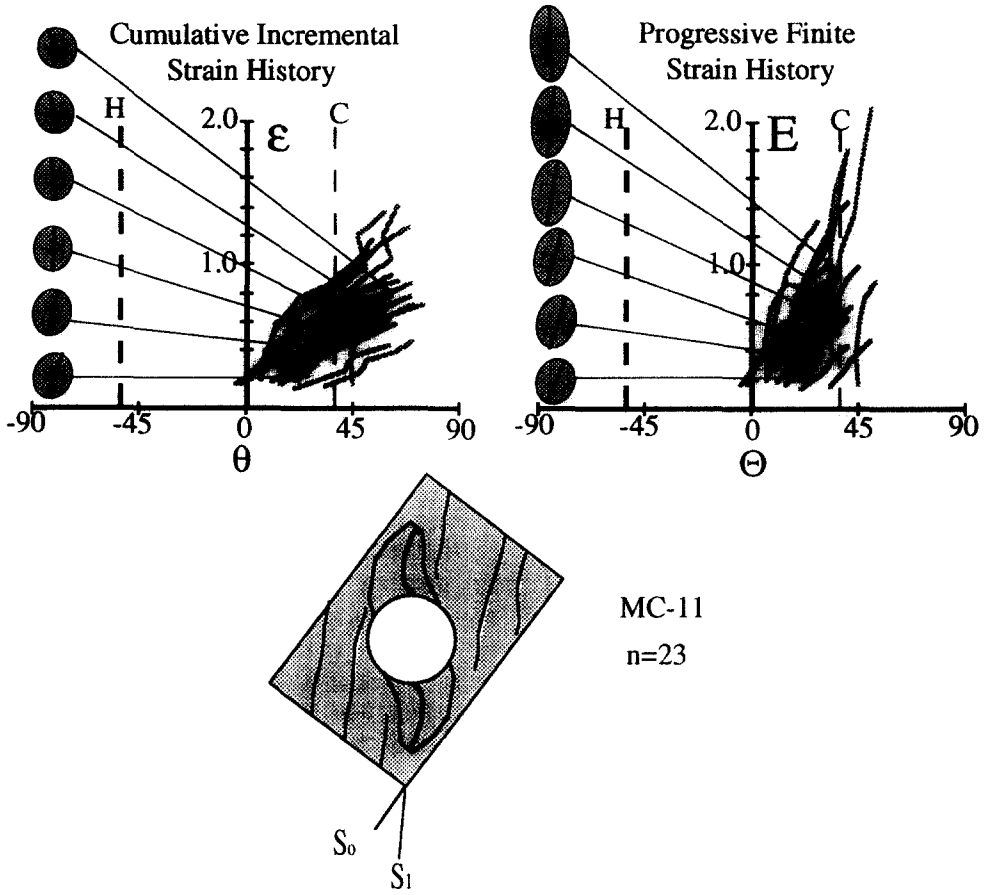

Fig. 7. Cumulative incremental strain history and progressive finite strain history plots. On each graph, extension is plotted vs orientation measured with respect to bedding with counterclockwise positive. Bold dashed line (marked H) represents horizontal and the fine dashed line (marked C) represents the trace of cleavage on the section. Gray curves plot data from an individual pressure shadow while the black curve is a plot of the average data for a sample. On the cumulative incremental strain history plot, ellipses represent the incremental strain ellipse for each increment with the final extension direction for each increment indicated by the major axis. Ellipses on progressive finite strain history plot represent the shape and orientation (major axis) of the finite strain ellipse after each increment. N = number of measured mineral fibers. One central fiber was measure from each pressure shadow.

as a reference frame for the extension direction. A horizontal reference frame and the orientation of cleavage, if present, are also shown. The cumulative incremental strain history depicts changes in the orientation of the incremental extension direction relative to these spatial reference frames (i.e. the final orientation of bedding, cleavage and horizontal) as strain accumulates (Fig. 7). The slope of the curve is a measure of the external vorticity, defined as the vorticity in a spatial reference frame (Means personal communication); a steep or near vertical slope reflects a constant orientation of extension, and a shallow or subhorizontal slope reflects a rigid-body rotation with little or no accumulation of strain. A change in slope represents a change in the radius of curvature along the fiber. Cumulative incremental strain histories are used in this study: (1) to determine the sense of the apparent reorientation of the extension direction; (2) to quantify the rate of rotation (i.e. the slope or one half the external vorticity) and the amount of rotation (relative to the final orientation of bedding) for individual samples; and (3) to compare these results for different lithologies and at different positions within the large-scale structure.

Progressive finite strain histories depict variations in the shape and orientation of the finite strain ellipse (assuming that there is no volume change, or $\varepsilon_3 = 1/\varepsilon_1$, see Wickham 1973). During non-coaxial strain histories, the finite elongation can decrease as a consequence of sequential increments of extension in disparate orientations. If there are distinct events in the cumulative incremental strain history (rigid-body rotation or sharp change in slope), the progressive finite strain history can be used to determine the orientation and shape of the finite strain ellipse at the time of the event. The orientation and shape of the finite strain ellipse is indicated by the final position of the progressive finite strain history (Fig. 7).

Strain histories for individual fibers are shown in light gray, while an 'average' history for each sample is shown by the bold curve. The average cumulative incremental strain history is constructed by normalizing each of the individual curves to the averages for the endpoints of all the curves (Clark *et al.* 1993). Each normalized curve is broken into discrete segments at closely spaced regular intervals by linear interpolation between adjacent points. An average curve is then calculated by averaging the individual normalized curves point by point. If there is an event that is common to all pressure shadows in a sample (e.g. a sharp change in fiber orientation), the curves can be normalized at this additional point. In

these cases, rigid-body rotations from individual pressure shadows are not smoothed out by the averaging process. Average progressive finite strain histories are constructed by superposition of the incremental stretch tensors along the average cumulative incremental strain history (e.g. Elliott 1972, Wickham 1973). These average strain histories allow an objective evaluation to be made of populations of curves and, in combination with the individual curves, provide a qualitative measure of the heterogeneity of strain at the scale of a thin section.

Strain analyses were completed on samples from both the Buck Creek and the Mahogany Creek exposures. Most samples from the Mahogany Creek section are from the same layer within the Bluebird Mountain Formation (except sample MC-14, which is from a coarser-grained layer within the Bluebird Mountain Formation that has a wider spaced cleavage and a larger bedding–cleavage angle). Strain histories from these samples are used to constrain the relationship between strain history and structural geometry in a single lithology. The samples from the Buck Creek section, which include examples from the Surrett Canyon, Bluebird Mountain and Snaky Canyon Formations, are used to evaluate the kinematics for a variety of lithologies and to determine how penetrative strain histories vary along strike within this large-scale leading edge fold.

RESULTS

Mahogany Creek section

The results of incremental strain analyses for the Mahogany Creek section are presented in Figs. 8 and 9. The cumulative incremental strain histories from the Bluebird Mountain Formation record external vorticity in all cases, with a counterclockwise rotation of the extension direction relative to the trace of bedding (Figs. 8 and 10). There are several important differences, however, between strain histories from different limbs of the large-scale fold. On the back limb, the incremental extension direction at the onset of deformation (θ_i) is 0–20° steeper than the trace of bedding (S_0), whereas the incremental extension direction at the completion of deformation (θ_f) is at 25–60° steeper than the bedding trace (Fig. 8). Sample MC-2, which is the sample farthest from both the hinge of the anticline and the fault surface, has a nearly coaxial strain history (~5° of counterclockwise rotation), with extension approximately 25° steeper than the bedding trace. Sample MC-14, in a coarse sandstone near the anticlinal hinge shows a small counterclockwise rotation, and θ_i and θ_f are steeper than in adjacent penetratively cleaved layers. Nearly all the back limb samples display concave down strain history curves, i.e. fibers have a smaller radius of curvature near the host–overgrowth interface. The total rotation, or $\theta_i - \theta_f$, is similar for all backlimb samples at ~40–50°. Based on the progressive finite strain histories, the orientation of finite elongation on the backlimb is steeper than bedding and steepens in relation to bedding as samples approach the hinge of the fold (Fig. 9). The magnitude of the elongation gradually increases with proximity to the hinge from ~0.4 in sample MC-2 to ~1.0 in other backlimb samples (Fig. 9).

At the hinge of the anticline, the orientation of incremental and finite extension directions (relative to bedding and horizontal) differ dramatically from backlimb samples (sample MC-15, Figs. 9 and 10). Many of the individual curves display an early coaxial strain accumulation, a sharp counterclockwise change in the orientation of incremental extension, and a late coaxial strain accumulation. Thus, during the construction of the average strain history, individual curves were normalized to the onset of rigid-body rotation in addition to the averages of (θ_i, ε_i) and (θ_f, ε_f), respectively. The average strain history is non-coaxial with a counterclockwise rotation of the incremental extension direction from 14° clockwise (relative to both bedding and horizontal) to 35° counterclockwise. Early coaxial deformation (near vertical strain history curve) is followed by counterclockwise rotation of the extension direction (shallow positive slope). The finite elongation direction in the hinge of the anticline is subhorizontal and approximately parallel to bedding. The magnitude of finite elongation or ε_f is ~1.6 (Fig. 9).

On the more steeply dipping (~60°) forelimb of the anticline, the initial orientation of extension varies from 35° near the hinge of the anticline (sample MC-16) to 75° clockwise at the midway point between the trace of the anticlinal and synclinal hinges (Figs. 8 and 10). The final orientation of incremental extension is nearly bedding-parallel ($\phi_f \sim 70°$) for all forelimb samples except MC-16. Midway between the trace of the anticlinal and synclinal hinges (samples MC-21 and 126), the individual strain history curves display an initial slope that shallows to near horizontal after a small accumulation of strain and then steepens during the latest strain increments (Fig. 8). The deformation in these samples is remarkably homogeneous, so the average curve depicts the shallow portion of the individual curves without normalization of these curves to the sharp bend in fibers. In these cases, the total rotation of the incremental extension direction is ~45–70°. The finite elongation direction is steeper than bedding on the forelimb, and the magnitude of elongation varies from a maximum of 1.0 near the hinge to a minimum of 0.4–0.6 midway between the trace of the anticlinal and synclinal hinges (Fig. 9).

At the hinge of the syncline (sample MC-27) and on the hanging wall flat forward of the anticline (samples 125 and 124), the initial incremental extension direction is inclined 25–40° clockwise relative to bedding ($\theta_i \sim -25$ to 40°) (Figs. 8 and 10). The extension direction gradually rotates ~45° counterclockwise, and the final orientation of incremental extension is inclined counterclockwise relative to bedding (θ_f ~20–30°) (Figs. 8 and 10). These samples display concave-down strain history curves similar to the backlimb samples. With the exception of sample MC-26 (from the vertical east limb of the small décollement fold within the Bluebird Mountain

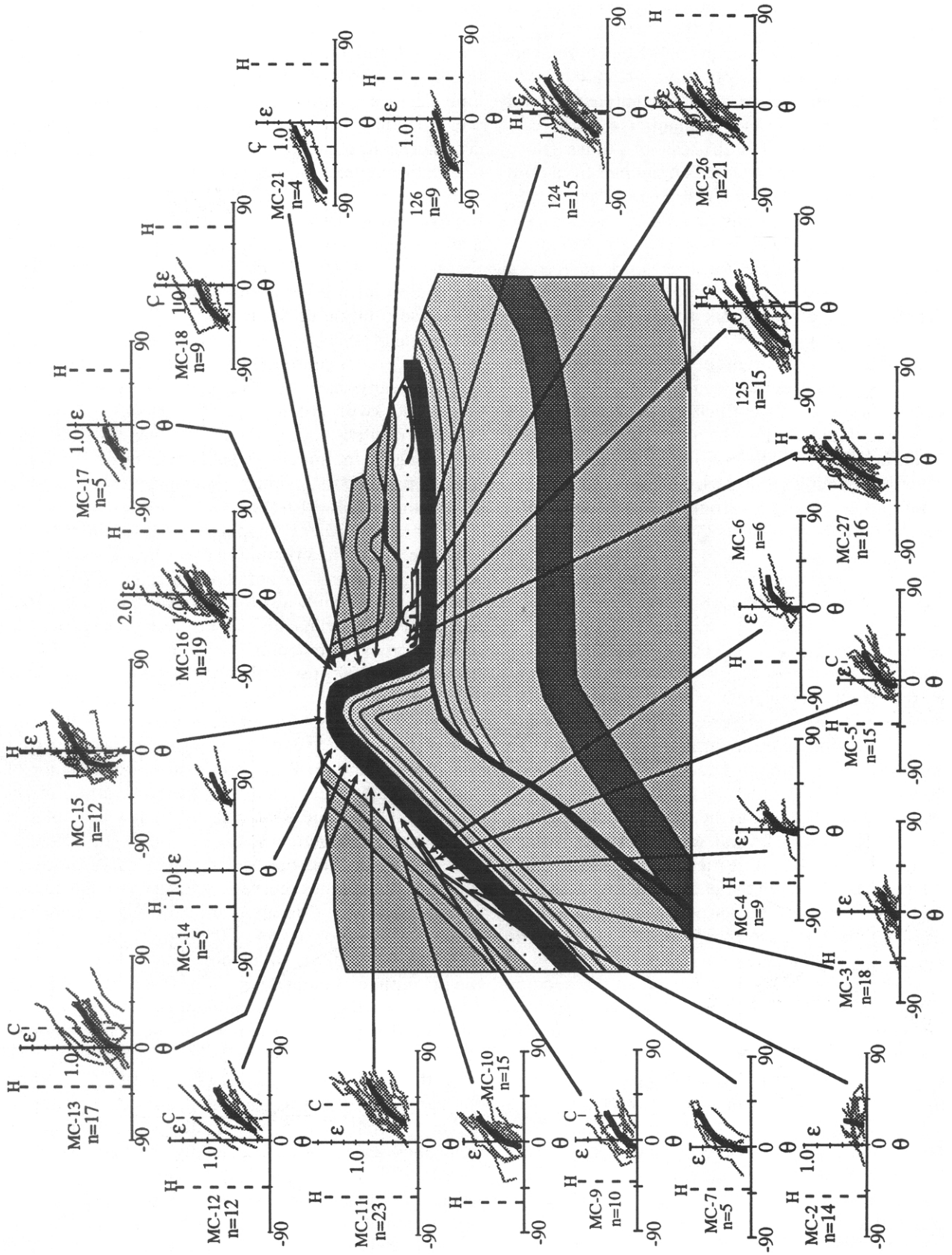

Fig. 8. Cumulative incremental strain history plots from Mahogany Creek samples. Patterning is the same as in Fig. 2 and reference frames are labeled the same as in Fig. 7.

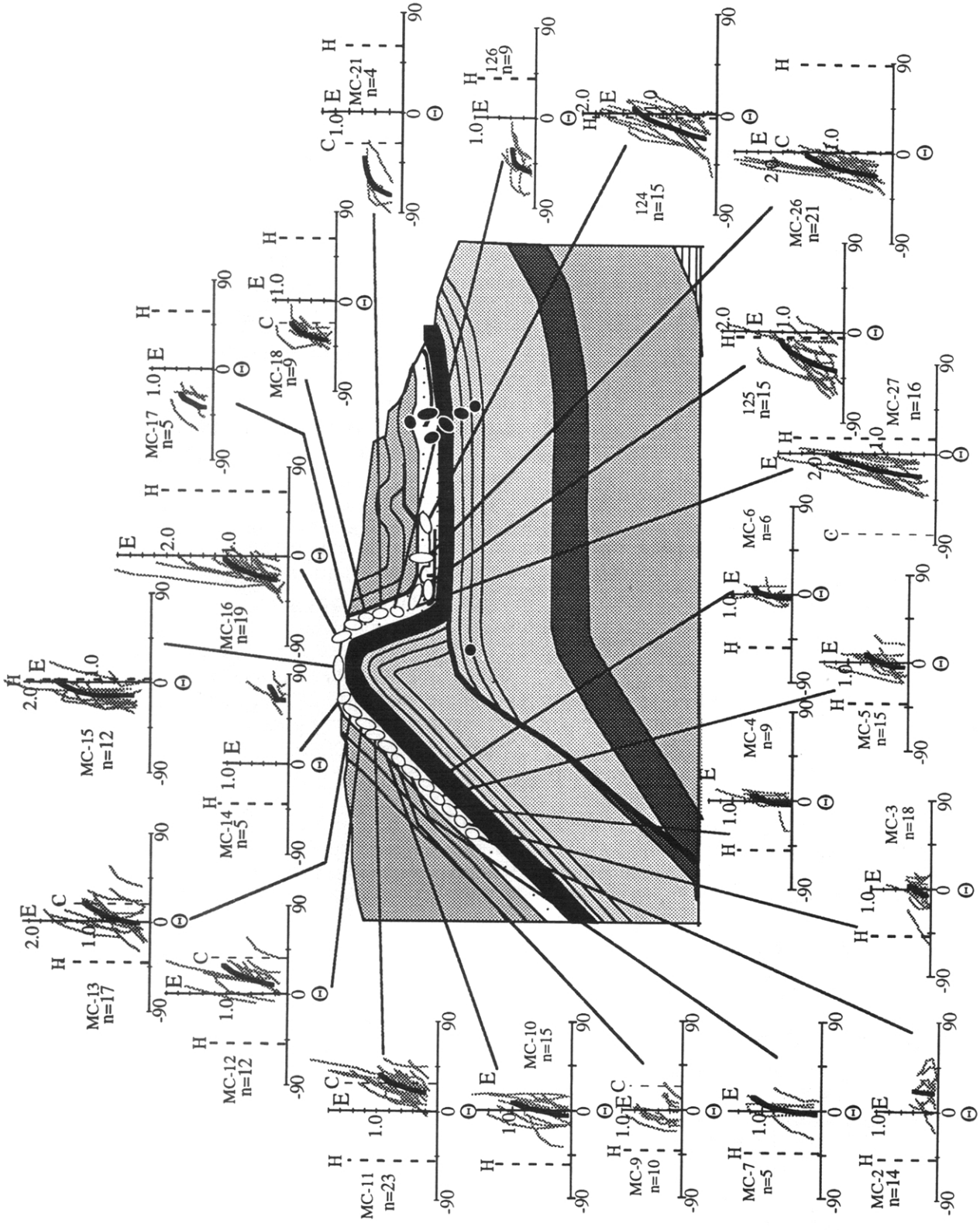

Fig. 9. Progressive finite strain history plots from Mahogany Creek samples. Sample locations marked by ellipses of appropriate final magnitude and orientation. White ellipses represent the finite strain recorded by incremental strain markers, black ellipses represent finite strain ellipses based on normalized grain center distributions (Erslev 1988) within oolites and calcareous siltstones that did not have overgrowths that were suitable for measurements of strain histories. Patterning is the same as in Fig. 4.

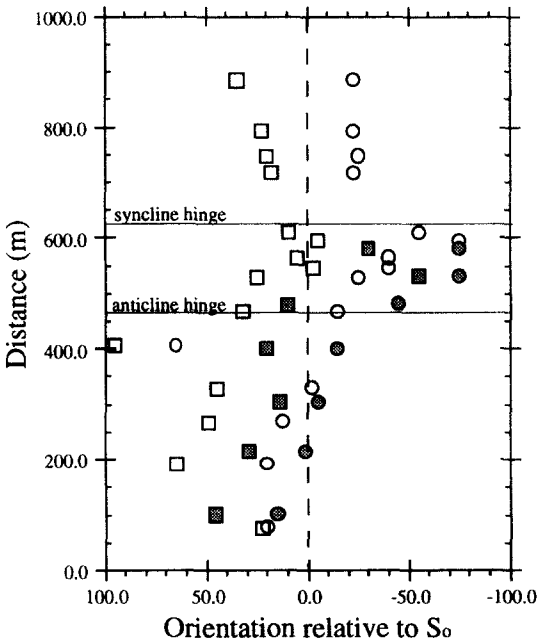

Fig. 10. Plot of initial (circles) and final (squares) extension directions relative to bedding vs distance parallel to bedding measured from an arbitrary position on the backlimb of the structure. Mahogany Creek and Buck Creek samples are represented by open and shaded symbols, respectively.

Formation), the finite elongation direction in hanging wall flat samples is subhorizontal or slightly inclined relative to the underlying bedding-parallel fault surface (Fig. 9). The magnitude of finite elongation varies from 1.05 to 1.75 (Fig. 9).

Buck Creek section

Along the Buck Creek section, strain histories also depict variations in the orientation of incremental extension relative to bedding (Fig. 11). While kinematic patterns resemble those from the Mahogany Creek section, there are some differences between the kinematics in different units. In individual beds within both the Bluebird Mountain and Surrett Canyon Formations, deformation was relatively homogeneous up to the scale of an entire fold limb but heterogeneous between adjacent beds and within individual beds from distinct structural positions (e.g. opposing fold limbs). Deformation within the Surrett Canyon Formation, for example, was localized into layer-parallel shear zones with a strongly developed nearly bedding-parallel cleavage, while the Bluebird Mountain Formation was penetratively deformed with cleavage consistently steeper than bedding.

Bluebird Mountain back limb samples (54, BC-5, BC-7 and BC-8) have an initial incremental extension direction that is nearly parallel to bedding but rotates gradually counterclockwise into a steeper orientation (Figs. 10 and 11). Bluebird Mountain forelimb samples (BC-11, BC-15 and BC-16) also record a counterclockwise rotation of the incremental extension direction, and with the exception of sample BC-12 have an initial extension direction oriented at very high angles to bedding. The final orientation of incremental elongation is nearly vertical and at smaller angles to bedding. The individual cumulative incremental strain curves and average incremental strain histories for these samples all display a steep initial segment followed by a shallower segment and a final steep segment (Fig. 11). The average strain history in sample BC-11 was the only curve normalized to the sharp bend in syntectonic fibers. Progressive finite strain histories in the Bluebird Mountain Formation are similar in the Buck Creek section to the results from the Mahogany section. With the exception of BC-5 on the backlimb, there is a gradual increase in the magnitude of finite elongation towards the hinge from values of ~0.4 to ~1.0 (Fig. 12).

Because overgrowths are rare within the massive beds of the Surrett Canyon Formation, all the measured strain histories from this unit are from the highly deformed, 5–10 m spaced, thin (0.1–0.5 m) clastic interbeds. In the hanging wall on the backlimb near the fault surface (samples 50, 51 and 33), the cumulative incremental strain histories are concave-down with a gradual counterclockwise rotation of the incremental extension direction into a steeper orientation than bedding (Fig. 11). In the hinge of the anticline (samples 55 and BC-9), the final orientation of incremental extension is nearly vertical and perpendicular to bedding. Sample 55 records a very slight clockwise rotation of a steep incremental extension direction throughout the history, whereas sample BC-9 (at the contact between the Arco Hills and Bluebird Mountain Formations) records a counterclockwise rotation of the incremental extension direction with only the final orientation of extension perpendicular to bedding (Fig. 11).

In the forelimb of the anticline in the Surrett Canyon Formation (sample BC-10), the cumulative incremental strain history displays a clockwise rotation of the incremental extension direction to ~25° clockwise relative to bedding. In the footwall of the thrust (samples 48 and 47), the strain is heterogeneous with both clockwise and counterclockwise rotations, but the incremental extension direction is in both cases oriented counterclockwise relative to bedding and steeper than ~30° throughout the history (Fig. 11). The magnitude of finite elongation in the Surrett Canyon Formation is greatest in the hanging wall near the fault surface and in the core of the anticline, with measurable footwall strain only observed near the fault surface. The orientation of finite elongation is near vertical in the hinge and inclined counterclockwise in all other samples (Fig. 12).

DISCUSSION

All the variations in the incremental extension direction depicted in Figs. 8 and 11 are with respect to geographic reference frames (horizontal and the orientations of cleavage or bedding). Thus, curved fibers provide a record of the external rotation, or the rotation with respect to these external or spatial reference frames. The external vorticity reflects a combination of the internal vorticity, or the rotation rate with respect to

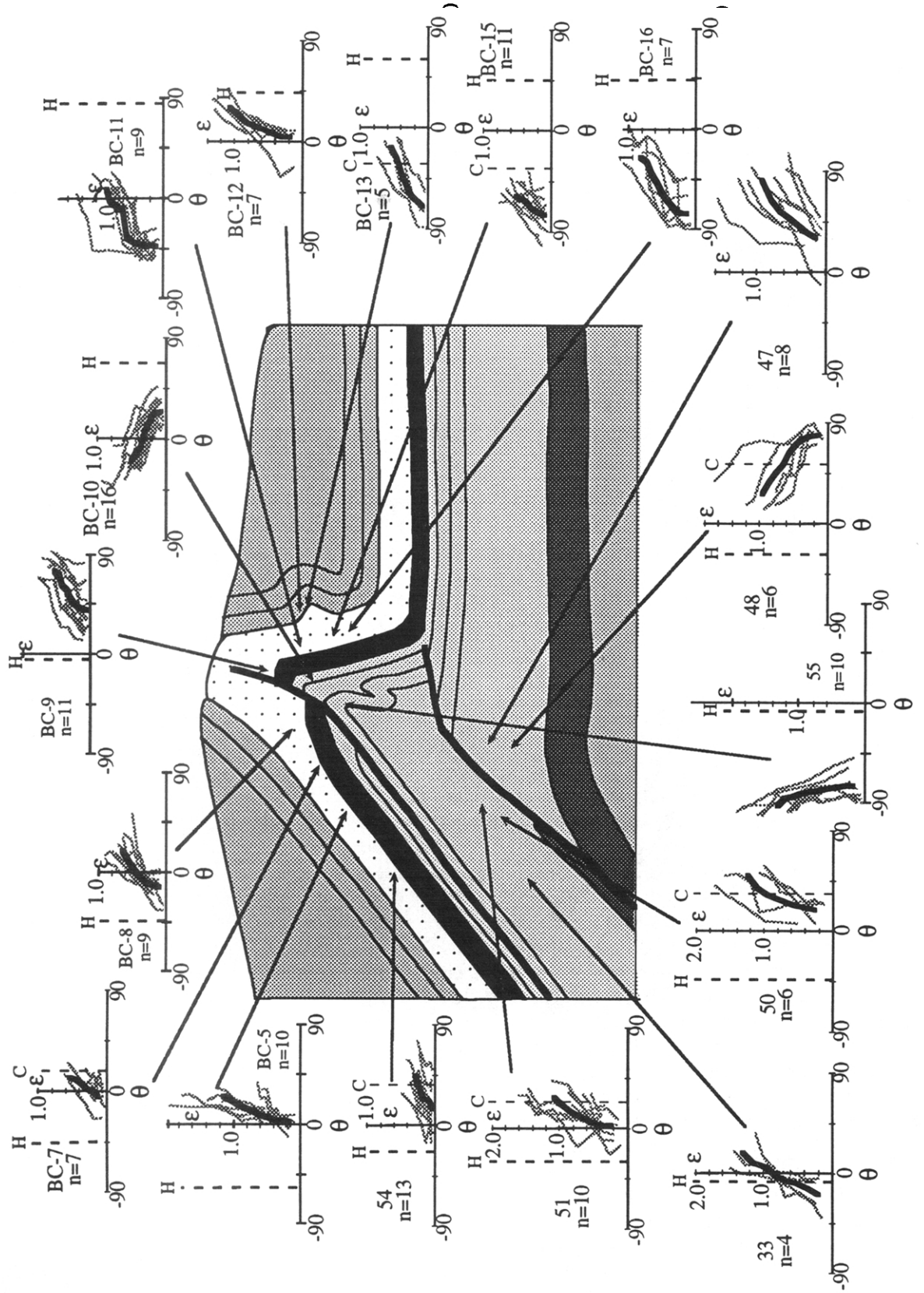

Fig. 11. Cumulative incremental strain history plots from Buck Creek samples. Patterning is the same as in Fig. 4 and reference frames are labeled the same as in Fig. 7.

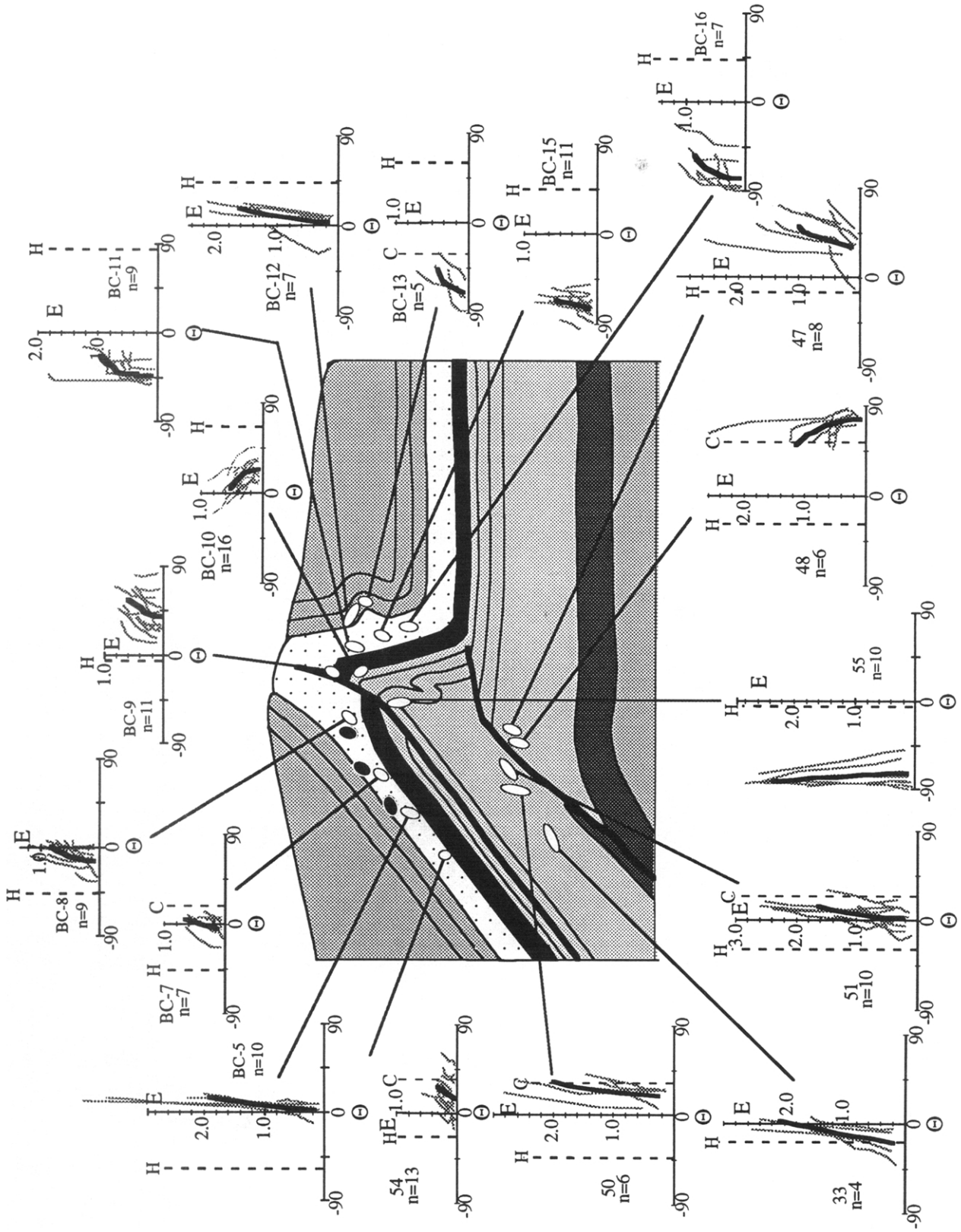

Fig. 12. Progressive finite strain history plots from Buck Creek samples. Sample locations marked by ellipses of appropriate final orientation and magnitude. White ellipses represent the finite strain recorded by incremental strain markers, black ellipses represent finite strain ellipses based on normalized grain center distributions (Erslev 1988) from calcareous siltstones that were suitable for measurements of strain histories. Patterning is the same as in Fig. 4.

a reference frame fixed to the incremental stretching directions, and the spin, or the body rotation rate, in a geographic reference frame (Means personal communication). For example, curved fibers in overgrowths on the limbs of folds can reflect a combination of simple shearing (internal vorticity) and limb rotation (spin). For a fold pinned in the hinge, the internal vorticity on fold limbs is opposite in sense to the spin. By examining the distribution of strain histories in a variety of spatial reference frames, we can assess the relative importance of these separate components for the external rotation recorded by curved fibers.

Simple shearing during fiber growth produces a gradual rotation of fibers that is synthetic with the sense of shear (Etchecopar & Malavieille 1987, Fisher & Byrne 1992). During folding, bedding-parallel simple shearing can be due to flexural-flow toward pin lines. It is important to note that fibers record the orientations of incremental extension relative to the final orientation of bedding and not relative to the orientation of bedding at the time of each increment of fiber growth. If the earliest-formed portion of fibers is rotated toward the shear direction, only the last increment of strain reflects the orientation of fiber *growth* relative to bedding. In the case of bedding-parallel simple shear, fibers should curve from near-parallel to bedding to inclined at 45° to bedding. The apparent rotation of the incremental extension direction with respect to spatial reference frames is due to rotation of material lines (i.e. fiber segments) through a fixed stretching direction and is therefore in an opposite sense as the sense of shear.

In the absence of internal vorticity, the fiber curvature reflects only the spin. On the limb of a fold, intrabed deformation may not involve internal vorticity if bedding-parallel faults allow interbed slip. During folding, beds may experience initial thickening followed by explosive fold amplification and finally, homogeneous shortening during interlimb tightening (Scott *et al.* 1965). Given a fixed vertical stretching direction, early-formed portions of fibers on a fold limb would be approximately perpendicular to bedding, but would curve into a steep orientation. A clockwise spin produces an apparent counterclockwise rotation of the extension direction with respect to a spatial reference frame.

The strain histories recorded by fibers are most likely contemporaneous with development of the Mahogany Creek–Buck Creek structure because strain histories relative to bedding differ for the different limbs of the structure. Moreover, the finite elongation directions from fibers are roughly parallel to the cleavage, which forms a divergent fan about the anticline. The similarity in shape and size of the cumulative incremental strain and progressive finite strain curves derived from individual pressure shadows (Figs. 8, 9, 11 and 12) indicates the homogeneity of the incremental and finite strains at the scale of a thin section. Given these considerations, the kinematics associated with different positions on the Mahogany Creek–Buck Creek structure can be reconstructed from the variations in incremental extension direction relative to spatial (i.e. bedding and horizontal) reference frames. For example, in the Bluebird Mountain Formation and in clastic interlayers of the Surrett Canyon, Snaky Canyon and Arco Hills Formations, the orientation of incremental extension in backlimb samples varies from initially bedding-parallel to moderately inclined relative to bedding (nearly vertical). Given that bedding on the backlimb is tilted ~50° counterclockwise relative to horizontal, it is unlikely that the counterclockwise rotation of the incremental extension direction (Figs. 8 and 11) is a consequence of a clockwise spin. We favor an interpretation for back limb strain histories that involves a component of bedding-parallel top-to-the-foreland (east) simple shearing because the earliest fiber segment is nearly bedding-parallel, whereas the latest fiber segment is inclined ~25–60° relative to bedding. These variations are consistent with progressive rotation of fiber segments toward bedding. The concave-down appearance of cumulative incremental strain histories could be accounted for by the fact that rate of rotation of an individual fiber segment in response to simple shearing decreases as the fiber approaches parallelism with the shear zone boundaries. Top-to-the-east simple shearing is consistent with flexural-flow during folding and/or deformation related to slip on the underlying fault surface.

On the forelimb of the anticline, cumulative strain histories for the Bluebird Mountain Formation display an initial extension direction at a high angle to bedding, progressive counterclockwise rotation of the extension direction, and a final extension direction that is steep and nearly bedding-parallel (Figs. 8 and 11). This strain history is inconsistent with bedding-parallel simple shearing because the final orientation of incremental extension is parallel to rather than inclined to bedding and the earliest portion of fibers is at a high angle to bedding. Moreover, a counterclockwise rotation of the incremental extension direction is the opposite sense of rotation predicted for a flexural-flow model with a pinned hinge. We interpret the counterclockwise rotation of the incremental extension direction as primarily a consequence of clockwise spin of the forelimb through a steep extension direction that is nearly fixed in a spatial reference frame. This model is consistent with the evidence for early extension at a high angle to bedding, a large rotation with little strain accumulation and late extension nearly parallel to bedding. The amount of rotation recorded by samples midway between anticlinal and synclinal hinges is similar to the limb rotation indicated by the bedding dip. Finally, the shape of most strain history curves on the Bluebird Mountain Formation forelimb (Figs. 8 and 11), with a slope that is steepest at the beginning and end of strain histories, is consistent with early subhorizontal shortening followed by rapid fold amplification and late interlimb tightening.

The strain history for the Bluebird Mountain Formation forelimb, with initial bed thickening and late bed

thinning, is remarkably similar to kinematic predictions based on area-balance models for the unfaulted layer of a fault propagation fold (Mitra 1990). For the observed interlimb angle, the area-balance model (Mitra 1990) is also consistent with the lack of significant finite extension or shortening perpendicular to bedding on the forelimb. For samples collected along the Bluebird Mountain Formation forelimb, the spin does not progressively occur later in the strain history (e.g. Beutner & Deigel 1985), so there is no clear evidence for forelimb growth by migration of either the synclinal or anticlinal axial surfaces (e.g. Suppe & Medwedeff 1990).

In clastic interlayers of the Surrett Canyon Formation, the only sample from the forelimb (sample BC-10) records an apparent clockwise rotation of the extension direction relative to bedding. For this sample, the final orientation of extension is parallel to the final orientation of extension in forelimb samples from the overlying Bluebird Mountain Formation, but the external vorticity involves rotation of an opposite sense. We interpret this result as an indication that, while the Bluebird Mountain Formation was experiencing clockwise spin through an externally fixed extension direction on the forelimb, the clastic interlayers of the Surrett Canyon Formation experienced layer-parallel simple shear with flexural-flow toward a pinned hinge.

Within the Bluebird Mountain Formation on the flat limb of the Mahogany section, just above the fault surface and near the tip line, strain histories also record a counterclockwise rotation of the incremental extension direction, but the initial orientation of incremental extension plunges east whereas the final orientation plunges west (Fig. 8). This strain history is inconsistent with spin through a fixed extension direction because, given the lack of stratigraphic separation on the underlying fault surface, bedding was horizontal throughout the development of the anticline. The flat limb strain histories are best explained by a bedding-parallel simple shear model which would account for apparent rotation of the incremental extension direction without any tilting of the rocks. Simple shearing would result in progressive clockwise rotation of early-formed fiber segments. The rotation of the earliest fiber segment through the shear plane is consistent with rigid fiber behavior. Finally, top-to-the-east simple shearing is consistent with proximity to the underlying E-directed thrust and the observation that finite elongations in the Bluebird Mountain Formation are greater on the flat limb than in other parts of the structure.

The kinematic model described above for each of the fold limbs on the Mahogany Creek–Buck Creek structure has implications for the positioning of pin lines, or lines of no intrabed shear or interbed slip. The difference in kinematics between the backlimb and the forelimb within the Bluebird Mountain Formation (flexural-flow on the backlimb that feeds forward into forelimb spin), for example, requires a pin somewhere on the forelimb (Fig. 1d). This is consistent with the observed strain histories for hinge samples from the Arco Hills and Bluebird Mountain Formations (BC-9 and MC-15), which record variations in the extension direction relative to bedding and horizontal reference frames (Figs. 8 and 11). MC-15 records an early coaxial strain accumulation at a low angle to bedding followed by a rapid change in the orientation of incremental extension. In the Surrett Canyon Formation, the reversal in sense of shear between backlimb and forelimb samples requires a pin near the hinge. A hinge sample (sample 55) in the Surrett Canyon Formation shows little rotation with near vertical extension and could be described as pinned. These results suggest that position of pin lines may vary as a function of lithology on the Mahogany Creek–Buck Creek structure and a pin line early in the deformation history can migrate within a layer as the structure evolves. A loose line on the backlimb within the Surrett Canyon Formation is stepped as a result of simple shear located in narrow zones (samples 33, 50 and 51), whereas a loose line in the Bluebird Mountain Formation is inclined hindward and more continuous with a steeper orientation in more competent layers (e.g. sample MC-14) (Fig. 13).

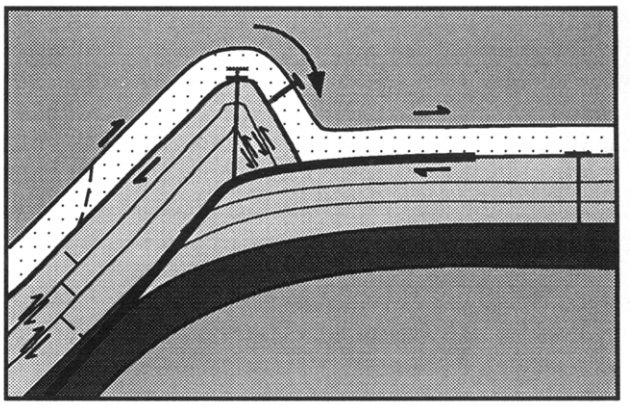

Fig. 13. Summary kinematic model for the development Mahogany Creek–Buck Creek structure showing pin lines (nails—black fixed, gray transient). The loose line (dashed) in the Bluebird Mountain Formation is from the Geiser *et al.* (1988) strain model with a pinned forelimb (Fig. 1d). Loose line in the Surrett Canyon Formation is from line length balances of photographs, sketches and cross-sections. Footwall pin is based on absence of strain in clastic interlayers.

The magnitude of finite elongation measured in samples from a single bed within the Bluebird Mountain Formation gradually increases along both the backlimb and the forelimb towards the hinge of the anticline (Fig. 9). One explanation for the variation in elongation toward the hinge is that there is large-scale redistribution of mass around the structure with volume loss farther from the hinge and volume gain near the hinge. We note that low strain samples such as MC-2 and MC-3 have similar cleavage intensity to higher strain samples closer to the hinge despite significantly different amounts of fibrous overgrowth material. Finite elongation on the flat limb above the fault surface is similar in magnitude to elongations near the hinge of the anticline (Fig. 9).

In the Bluebird Mountain Formation, the orientation of finite elongation is steeper than bedding on the backlimb and forelimb of the anticline and nearly paral-

lel to the bedding on the front flat limb. In the hinge of the anticline, the finite elongation direction is subhorizontal and nearly parallel to bedding. The distribution of elongation directions on the anticline reflect the divergent fanning cleavage within the Bluebird Mountain Formation above the more competent Surrett Canyon Formation. Subhorizontal extension in the hinge may be a consequence of the lack of slip between the weak Bluebird Mountain Formation and the outer arc of a massive bed at the top of the Arco Hills Formation. In the Surrett Canyon Formation, the finite elongation direction is nearly vertical in the hinge of the anticline and fault-parallel in deformed layers from the footwall and hanging wall near the fault.

Strain histories in the Bluebird Mountain Formation display many similarities between the Buck Creek and Mahogany Creek sections, such as evidence for bedding-parallel simple shearing on the back limb and clockwise rotation relative to a fixed extension direction on the forelimb. The main difference in strain histories between the two sections is that there is less total rotation in samples from the Buck Creek section, an observation that is consistent with the shallower bed dips and smaller interlimb angle. The geometry of the anticline is similar in both sections, suggesting the possibility of time–space equivalence with northward self-similar fault and fold propagation (e.g. Elliott 1976). Whether or not fault propagation and folding develops self similarly within a given thrust system (e.g. Elliott 1976, Knipe 1989), likely depends on rheology (Fischer & Woodward 1992), lateral stratigraphic variations (Rich 1934), position along the tip line (dislocation type) or variations in transport direction within a thrust sheet. The similar geometry and hanging wall strain histories between the Mahogany Creek and Buck Creek sections suggests that folding and penetrative strain in the hanging wall of the fault occurred above the ramp prior to the existence of the upper flat. The anticline was subsequently transported along the upper flat without major modification in fold geometry or hanging wall strain distribution.

One explanation for self-similar fold development is that the fold and fault are geometrically linked, with migration of the synclinal axial surface with the thrust tip line (Suppe & Medwedeff 1990). An alternative possibility that is consistent with observations in this and other studies (e.g. Fischer *et al.* 1992) of fixed anticlinal and synclinal axial surfaces is that folding and faulting are independent competing mechanisms of shortening that interact mechanically rather than geometically. Initial ramp propagation is accompanied by development of a buckling instability in the hanging wall. Because buckling is followed by explosive fold amplication at a lower differential stress, strike-parallel and forward ramp propagation may be blunted by the fold-accommodated shortening and, in the case of the Buck Creek section, by footwall shortening. Once the fold tightens to its present geometry and fold shortening requires a greater differential stress, forward fault propagation resumes as it did along the Mahogany Creek section, transporting the anticline onto the upper flat.

CONCLUSIONS

The Mahogany Creek–Buck Creek structure within the Lost River Range, Idaho, is a large-scale, leading edge fold which developed in late Paleozoic outer shelf stratigraphy during the Sevier orogeny. The leading edge of the thrust fault is exposed in two transverse valleys which show from south to north: (1) a decrease in thrust displacement; (2) a decrease in the amount of total shortening; and (3) a decrease in stratigraphic separation; all of which suggests a northward propagating thrust tip line. Incremental strain histories determined from antitaxial fibrous overgrowths in pressure shadows quantify temporal variations in the magnitude and orientation of elongation as a function of the well-constrained structural geometry and provide a basis for kinematic analysis of fault propagation folding. Ubiquitous coaxial up-dip extension on axial surface-parallel cleavage planes record plane strain deformation.

On the backlimb of the structure, the Bluebird Mountain Formation, a fine-grained calcareous sandstone, deformed by bed-parallel flexural-flow, whereas the forelimb of the structure records a clockwise spin of bedding through a nearly fixed, steeply plunging incremental extension direction. The flat limb ahead of the large-scale anticline exhibits top to-the-foreland (east) simple shearing related to slip on the underlying fault. In contrast, the underlying Surrett Canyon Formation, a massive carbonate, experienced hingeward-directed flexural-flow localized within thin clastic interbeds on both limbs of the anticline. Incremental strain histories in samples from the hinge zone around the structure suggest a kinematic partitioning between pin lines which were variably distributed within each unit, and which were in part transient. Finite elongations are greatest in the hinge area and above the foreland flat in the Bluebird Mountain Formation. They are negligible in the Surrett Canyon Formation except within the mechanically active clastic interbeds of the hanging wall and at the pinned anticlinal hinge in the footwall. Comparison of the Mahogany Creek and Buck Creek sections suggests contemporaneous folding and strike-parallel ramp propagation with forward thrust propagation blunted by the fold-accommodated shortening. Once the fold tightened and fold shortening required a greater differential stress, forward fault propagation resumed, transporting the anticline onto the upper flat.

Acknowledgements—This research was supported by a collaborative NSF Grants EAR9018433 awarded to D. M. Fisher and EAR9017334 awarded to D. J. Anastasio and a National Geographic grant awarded to D. J. Anastasio and D. M. Fisher. The paper was improved based on comments from C. Hedlund, G. Mitra, S. Wojtal and an anonymous reviewer. We would also like to acknowledge S. Janecke for discussions about the stratigraphy within the Lost River Range and W. Means for helpful discussions about kinematics and for providing us with a preprint of a manuscript in preparation. We thank V. Johnson and the people of Mackay, Idaho for logistical support throughout this study.

REFERENCES

Beutner, E. C. & Diegel, F. A. 1985. Determination of fold kinema-

tics from syntectonic fibers in pressure shadows, Martinsburg slate, N. J. *Am. J. Sci.* **285**, 16–50.
Boyer, S. E. 1986. Styles of folding within thrust sheets: examples from the Appalachians and the Rocky Mountains of the U.S.A. and Canada. *J. Struct. Geol.* **8**, 325–339.
Boyer, S. E. & Elliott, D. 1982. Thrust systems. *Bull. Am. Ass. Petrol. Geol.* **66**, 1196–1230.
Chapman, T. J. & Williams, G. D. 1984. Displacement–distance methods in the analysis of fold-thrust structures and linked-fault systems. *J. geol. Soc. Lond.* **141**, 121–128.
Clark, M. B., Fisher, D. M. & Chia-yu, L. 1993. Kinematic analysis of the Hfueshan Range: A large-scale pop-up structure. *Tectonics* **12**, 205–217.
Dahlstrom, C. D. A. 1970. Structural geology in the eastern margin of the Canadian Rocky Mountains. *Bull. Can. Petrol. Geol.* **18**, 332–406.
Douglas, R. J. W. 1958. Mount head map-area, Alberta. *Mem. geol. Soc. Can.* **291**.
Durney, D. W. & Ramsay, J. G. 1973. Incremental strains measured by syntectonic crystal growth. In: *Gravity and Tectonics* (edited by DeJong, K. A.). Wiley, New York, 67–96.
Elliott, D. 1972. Deformation paths in structural geology. *Bull. geol. Soc. Am.* **83**, 2621–2638.
Elliott, D. 1976. The energy balance and deformation mechanisms of thrust sheets. *Phil. Trans. R. Soc. Lond.* **A283**, 289–312.
Erslev, E. A. 1988. Normalized center-to-center strain analysis of packed aggregates. *J. Struct. Geol.* **10**, 201–209.
Etchecopar, A. & Malavieille, J. 1987. Computer models of pressure shadows: a method for strain measurement and shear-sense determination. *J. Struct. Geol.* **9**, 667–677.
Fischer, M. P. & Woodward, N. B. 1992. The geometric evolution of foreland thrust systems. In: *Thrust Tectonics* (edited by McClay, K. R.). Chapman & Hall, London, 181–189.
Fischer, M. P., Woodward, N. B., & Mitchell, M. M. 1992. The kinematics of break-thrust folds. *J. Struct. Geol.* **14**, 451–460.
Fisher, D. & Byrne, T. 1992. Strain variations in an ancient accretionary complex: implications for forearc evolution. *Tectonics* **11**, 330–347.
Geiser, J., Geiser, P. A., Kligfield, R., Ratliff, R. & Rowan, M. 1988. New applications of computer-based section construction: Strain analysis, local balancing, and subsurface fault prediction. *Mountain Geolog.* **25**, 47–59.
Geiser, P. A. 1988. Mechanisms of thrust propagation: some examples and implications for the analysis of overthrust terranes. *J. Struct. Geol.* **10**, 829–845.
Jamison, W. R. 1987. Geometric Analysis of fold development in overthrust terranes. *J. Struct. Geol.* **9**, 207–219.
Janecke, S., Geissman, J. & Bruhn, R. 1991. Localized rotation during Paleogene extension in east central Idaho, Paleomagnetic and geologic evidence. *Tectonics* **10**, 403–432.
Janecke, S. U. 1989. Changing extension directions from Eocene to present, central Lost River Range and adjacent areas, Idaho. *Geol. Soc. Am. Ab. w. Prog.* **21**, 97–98.
Knipe, R. J. 1989. Deformation mechanisms—recognition from natural tectonites. *J. Struct. Geol.* **11**, 127–146.
Link, P. K., Skipp, B., Hait, M. H., Janecke, S. & Burton, B. R. 1988. Structural and stratigraphic transect of south-central Idaho: a field guide to the Lost River, White Knob, Pioneer, Boulder, and Smoky Mountains. In: *Guidebook to the Geology of Central and Southern Idaho* (edited by Link, P. K. & Hacket, W. R.). *Bull. Idaho Geol. Surv.* **27**, 5–42.
Mamet, B. L., Skipp, B., Sando, W. J. & Mapel, J. 1971. Biostratigraphy of upper Mississippian and associated Carboniferous rocks in south-central Idaho. *Bull. Am. Ass. Petrol. Geol.* **55**, 20–33.
Mapel, W. J., Read, W. H. & Smith, R. K. 1965. Geologic map and sections of the Doublespring Quadrangle, Custer and Lemhi counties, Idaho. *U.S. geol. Surv. Map* **GQ-464**.
Mitra, G., Hull, J. M., Yonkee, W. & Protzman, G. M. 1988. Comparison of mesoscopic and microscopic deformation styles in the Idaho–Wyoming thrust belt and Rocky Mountain foreland. *Mem. geol. Soc. Am.* **171**, 119–141.
Mitra, S. 1990. Fault propagation folds: geometry, kinematic evolution, and hydrocarbon traps. *Bull. Am. Ass. Petrol. Geol.* **74**, 921–945.
Namson, J. 1981. Structure of the Western Foothills Belt, Miaoli-Hsinchu area, Taiwan: (1) southern part. *Petrol. Geol. Taiwan* **18**, 31–51.
Ramsay, J. G. & Huber, M. I. 1987. *The Techniques of Modern Structural Geology, Volume 2: Folds and Fractures*. Academic Press, New York.
Rich, R. L. 1934. Mechanics of low-angle overthrust faulting as illustrated by Cumberland thrust block, Virginia, Kentucky and Tennessee. *Bull. Am. Ass. Petrol. Geol.* **18**, 1584–1596.
Rose, P. R. 1977. Mississippian carbonate shelf margins, western United States. In: *Wyoming Geological Association Twenty-ninth Annual Field Conference* (edited by Heisey, E. L., Norwood, E. R. & Wach, L. A.), 155–172.
Ross, C. P. 1947. Geology of the Borah Peak quadrangle, Idaho. *Bull. geol. Soc. Am.* **58**, 1085–1160.
Ruppel, E. T. & Lopez, D. A. 1984. The thrust belt in southwest Montana and east-central Idaho. *Prof. Pap. U.S. geol. Surv.* **1278**, 1–41.
Sandberg, C. A. 1975. McGowan Creek Formation, new name for lower Mississippian flysch sequence in east-central Idaho. *Bull. U.S. geol. Surv.* **1405-E**, E1–E11.
Sandberg, C. A., Gutschick, R. C., Johnson, J. G., Poole, F. G. & Sando, W. J. 1982. Middle Devonian to late Mississippian geologic history of the overthrust belt region, western United States. In: *Geologic Studies of the Cordilleran Thrust Belt* (edited by Powers, R. B.). *Rocky Mountain Ass. Geol.* **2**, 691–719.
Scott, W. H., Hansen, E. & Twiss, R. J. 1965. Stress analysis of quartz deformation lamellae in a minor fold. *Am. J. Sci.* **263**, 729–746.
Skipp, B., Hoggan, R. D., Schleicher, A. & Douglas, R. C. 1979a. Upper Paleozoic carbonate bank in east-central Idaho—Snaky Canyon, Bluebird Mountain, and Arco Hills Formations and their paleotectonic significance. *Bull. U.S. geol. Surv.* **1486**.
Skipp, B., Sando, W. J. & Hall, W. E. 1979b. The Mississippian and Pennsylvanian systems in the United States—Idaho. *Prof. Pap. U.S. geol. Surv.* **1110-AA**, AA1–AA42.
Skipp, B. & Hait, M. H., Jr. 1977. Allochthons along the northeast margin of the Snake River Plain, Idaho, In: *Wyoming Geological Association Twenty-ninth Annual Field Conference Guidebook* (edited by Heisey, E. L., Norwood, E. R. & Wach, L. A.), 499–515.
Spencer, S. 1991. The use of syntectonic fibers to determine strain estimates and deformation paths: an appraisal. *Tectonophysics* **194**, 13–34.
Spratt, D. A. 1987. Finite strain and deformation mechanisms in carbonate thrust sheets. Unpublished Ph.D. dissertation, Johns Hopkins University, Baltimore, Maryland.
Suppe, J. 1983. Geometry and kinematics of fault-bend folding. *Am. J. Sci.* **283**, 648–721.
Suppe, J. & Medwedeff, D. A. 1990. Geometry and kinematics of fault propagation folding. *Eclog. geol. Helv.* **83**, 409–454.
Wickham, J. S. 1973. An estimate of strain increment in a naturally deformed carbonate rock. *Am. J. Sci.* **273**, 23–47.
Wojtal, S. & Mitra, G. 1988. Nature of deformation in some fault rocks from Appalachian thrusts. In: *Geometries and Mechanisms With Special Reference to the Appalachians* (edited by Mitra, G. & Wojtal, S.). *Spec. Pap. geol. Soc. Am.* **222**, 17–34.